

HU-EP-07/42

Smearing and filtering methods in lattice QCD — a quantitative comparison *

Stefan Solbrig^{†‡}

Universität Regensburg, Institut für Physik, 93040 Regensburg, Germany

E-mail: stefan.solbrig@physik.uni-regensburg.de

Falk Bruckmann

Universität Regensburg, Institut für Physik, 93040 Regensburg, Germany

E-mail: falk.bruckmann@physik.uni-regensburg.de

Christof Gattringer

Universität Graz, Institut für Physik, 8010 Graz, Austria

E-mail: christof.gattringer@uni-graz.at

Ernst-Michael Ilgenfritz

Humboldt-Universität zu Berlin, Institut für Physik, Newtonstrasse 15, 12489 Berlin, Germany

E-mail: ilgenfri@physik.hu-berlin.de

Michael Müller-Preussker

Humboldt-Universität zu Berlin, Institut für Physik, Newtonstrasse 15, 12489 Berlin, Germany

E-mail: mmp@physik.hu-berlin.de

Andreas Schäfer

Universität Regensburg, Institut für Physik, 93040 Regensburg, Germany

E-mail: andreas.schaefer@physik.uni-regensburg.de

We systematically compare three filtering methods used to extract topological excitations from lattice gauge configurations, namely smearing, Laplace filtering and the filtered fermionic topological charge (with chirally improved fermions). Each of these techniques introduces ambiguities, like its parameter dependence. We show, however, that all these methods can be tuned to each other over a broad range of filtering levels and that they reveal very similar topological structures. For these common structures we find an interesting power-law relating the number and packing fraction of clusters of filtered topological charge.

The XXV International Symposium on Lattice Field Theory

July 30 - August 4, 2007

Regensburg, Germany

*This work was supported by DFG under contract FOR 465.

We like to thank the Leibniz Rechenzentrum in Munich for support and training.

[†]Speaker.

[‡]supported by DFG and BMBF

1. Introduction

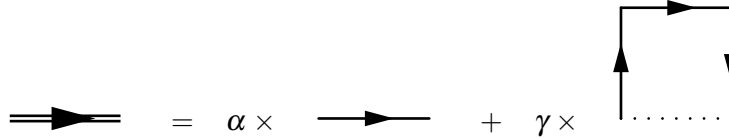
Topological objects are known to be linked to chiral symmetry breaking. They may also have a close connection with confinement. Therefore, the study on the lattice of how the topological charge is distributed in space-time will deepen the insight in those mechanisms. However, there is no unique topological charge density on the lattice. Various methods to define it on lattice gauge configurations exist, but they need not to agree on a given configuration. Filtering techniques are necessary to extract a smooth topological density that could eventually be interpreted in terms of continuum objects. In the talk we have discussed and compared filtering via smearing, Laplacian eigenmodes and Dirac eigenmodes, as in [1]. Preliminary results were presented in [2]. Our objective is to combine filtering methods in order to reduce ambiguities and highlight structures that are important at a certain level of smoothing.

Throughout this paper, we employ the *highly improved field strength tensor* [3] which uses a weighted clover average of 1×1 , 2×2 and 3×3 -plaquettes. With its help a gluonic definition of the topological charge density can be given, that yields, for typical Monte Carlo configurations, integer topological charge with good precision after few smearing steps. The configurations for zero temperature are 16^4 lattices generated with tree-level improved Lüscher-Weisz action at $\beta = 1.95$.

2. Filtering techniques

2.1 Smearing

Smearing is a gauge covariant local averaging for the gauge field in order to remove UV fluctuations. Every gauge link is replaced by a weighted average of the link itself and the sum of the bypassing staples. The resulting average needs to be projected back to the gauge group. The following diagram, sequentially applied to all links, visualizes one smearing step:



We used $\alpha = 0.55$, $\gamma = 0.075$ in all cases, following [4]. The smearing procedure is normally repeated several times to get stronger filtering, i.e., smoother configurations. The filtered topological charge is $q(x)$ computed from the smeared gauge fields using the improved field strength tensor:

$$q^{\text{smeared}}(x) = \frac{1}{16\pi^2} \text{tr} \sum_{\mu, \nu} \left[F_{\mu\nu}(x) \tilde{F}_{\mu\nu}(x) \right] \quad \text{with } F \text{ computed on smeared links.} \quad (2.1)$$

2.2 Laplace filtering

The eigenmodes of the lattice Laplacian can also be used as a low-pass filter for the gauge links [5]. This filter, however, is non-local. The lattice Laplacian

$$\Delta_{xy}^{ab} = \sum_{\mu=1}^4 \left[U_{\mu}^{ab}(x) \delta_{x+\hat{\mu},y} + U_{\mu}^{\dagger ab}(y) \delta_{x-\hat{\mu},y} - 2\delta_{ab} \delta_{xy} \right] \quad (2.2)$$

contains the original links, that can be reconstructed if all eigenmodes of (2.2) are known. For filtering, we truncate the sum in

$$U_\mu^{ab \text{ Laplace filtered}}(x) = - \sum_{n=1}^N \lambda_n \phi_n^a(x) \phi_n^{*b}(x + \hat{\mu}) \Big|_{\text{normalization}} \quad (2.3)$$

with $N \ll 2V$ with V being the lattice volume. If $N = 2V$, the formula is exact and the filtered gauge links would be identical to the original links. The topological charge is then computed via the improved field strength tensor on a configuration of Laplace filtered links, analogous to Eq. (2.1).

2.3 Dirac filtering

The third possibility to obtain a filtered topological charge density is to use eigenmodes of a chiral Dirac operator. We chose the *chirally improved* (CI) Dirac operator D^{CI} [6, 7]. Its eigenmodes are reasonably chiral, but the required computing time is much less than, e.g., for the overlap operator. The topological density $q(x)$ can be directly reconstructed from the eigenmodes, e.g., truncated to N pairs of non-zero modes:

$$\begin{aligned} q_N^{\text{rec.}}(x) = & \sum_{\substack{i=1 \\ \lambda_i \text{ complex}}}^N \left(\left(\frac{\lambda_i}{2} - 1 \right) \phi_{\lambda_i}^\dagger(x) \gamma_5 \phi_{\lambda_i}(x) + \left(\frac{\bar{\lambda}_i}{2} - 1 \right) \phi_{\bar{\lambda}_i}^\dagger(x) \gamma_5 \phi_{\bar{\lambda}_i}(x) \right) \\ & + \sum_{\text{all real } \lambda_j} \left(-\frac{1}{|\rho_{5,\lambda_j}|} \phi_{\lambda_j}^\dagger(x) \gamma_5 \phi_{\lambda_j}(x) \right) \text{ with } \rho_{5,\lambda_j} = \sum_x \left(\phi_{\lambda_j}^\dagger(x) \gamma_5 \phi_{\lambda_j}(x) \right) \end{aligned} \quad (2.4)$$

The eigenmodes are defined as $D^{CI} \phi_n = \lambda_n \phi_n$, such that λ is complex in general. The real modes determine the topological charge through the Atiyah-Singer index theorem.

Figure 1 visualizes the filtering methods by displaying the charge density over slices of the lattice. It shows a very good agreement of the various methods. Similar observations have been made in [8]. We want to emphasize that the agreement of the three methods is nontrivial since the methods differ profoundly.

3. Optimal filtering

Optimal filtering is a way to match the three filter parameters – the number of Dirac modes, of Laplace modes and of smearing steps – in such a way, that the resulting topological charge density obtained by either of the methods resembles the topological charge density obtained by the other methods. We consider the correlators and cross correlators $\chi_{q_A q_B}(r)$ of the topological charge densities q_A, q_B filtered with filter A and B . Then the relative normalization factor

$$\Xi_{q_A q_B} \equiv \frac{\langle \chi_{q_A q_B}(0) \rangle \langle \chi_{q_A q_B}(0) \rangle}{\langle \chi_{q_A q_A}(0) \rangle \langle \chi_{q_B q_B}(0) \rangle} \quad \text{with} \quad \chi_{q_a q_b}(0) \equiv (1/V) \sum_x q_a(x) q_b(x) \quad (3.1)$$

is a measure of the similarity of the topological charge densities q_A, q_B . Two filtered configurations are the more similar, the closer Ξ is to 1.

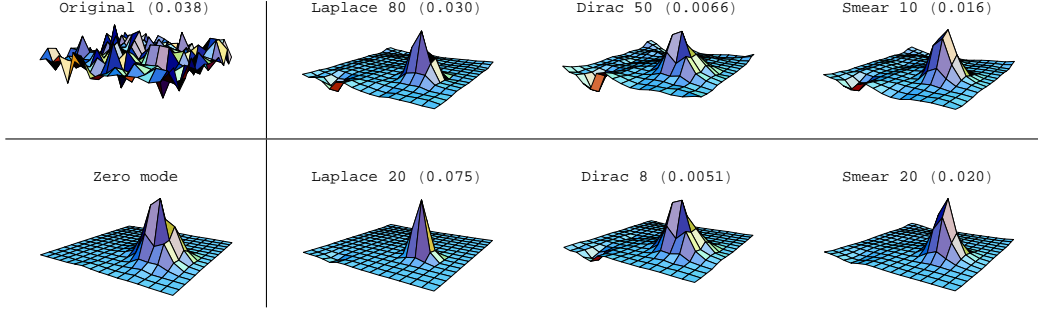


Figure 1: The plots visualize the filters. All images show the same 2-dimensional slice of the topological charge density of the same configuration. The upper left plot shows the unfiltered density. The lower left plot shows the scalar density of the single real eigenmode for comparison. The other plots show the filtered topological charge with the three methods and various filtering parameters. Note that the plots are drawn not in the same scale. Peak values are indicated in brackets.

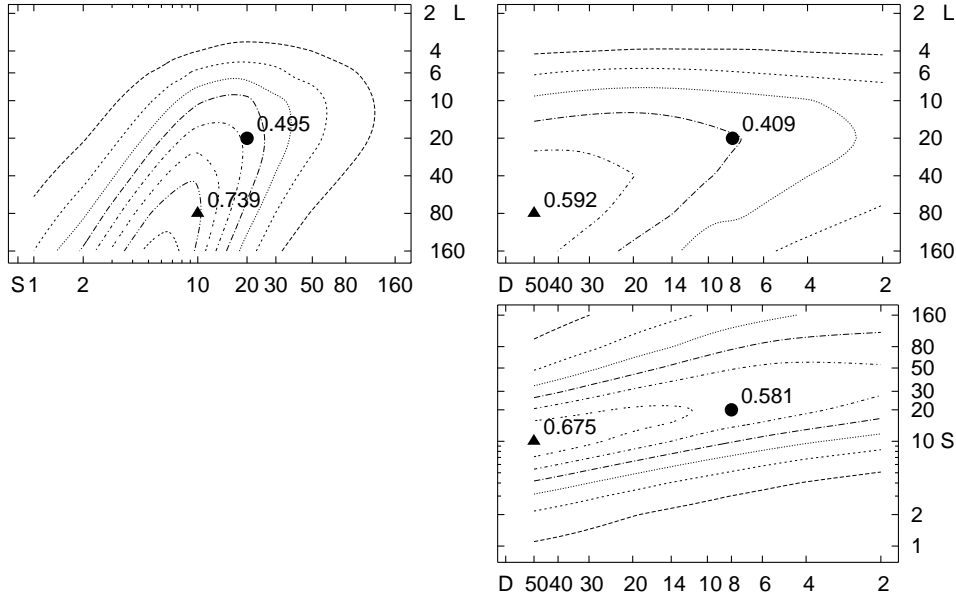


Figure 2: These plots show a pairwise comparison of filtering methods. Shown are lines of constant Ξ , as defined in Eq. (3.1). L, D and S refer to Laplace and Dirac filtering and smearing. The ridges in each contour plot represent the optimal matching between two methods. The triangle \blacktriangle denotes an example of weak filtering, the dot \bullet represents a case of strong filtering in all three methods. The dots in the right plots relate 20 Laplacian modes to 8 pairs of non-zero Dirac modes, and these to 20 smearing steps. The dot in the left plot is close to the ridge there, confirming the consistency of matching between all three methods.

4. Clusters

Once we have computed the topological charge density, we can try to identify individual objects. It is well known that the topological charge in smoothed configurations shows a “lumpy” structure.

We characterize a certain cluster state in different lattice configurations using a running “watermark” f rather than using a cutoff q_{cut} . This means that the lower cutoff q_{cut} in $|q(x)|$ for sites

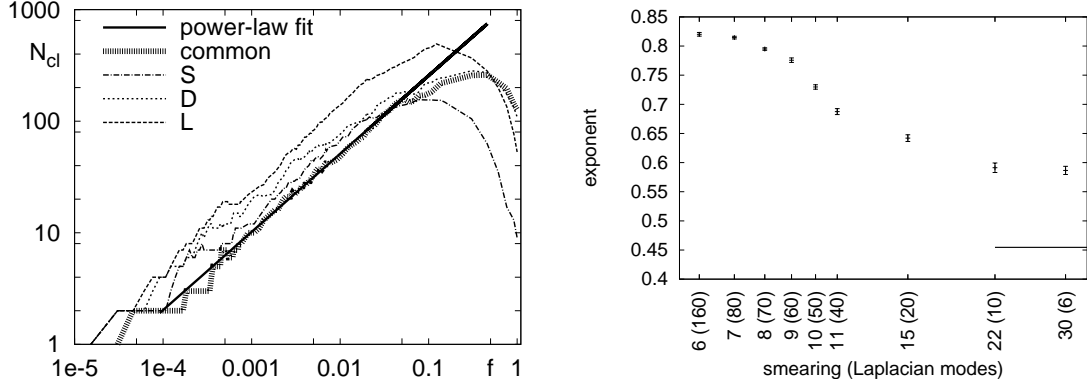


Figure 3: The left, double-log plot shows the number of clusters vs. the packing fraction f for various filtering methods. Note that for the thick, dotted line (labelled “common”) the linear regime is wider than for the individual filtering methods. This plot uses weak filtering, i.e., 10 smearing steps, 80 Laplace modes and 50 Dirac modes. The right hand side plot shows the exponent of the power law, obtained when only clusters are taken into account found by both smearing and Laplace filtering. The abscissa of the r.h.s. plot describes the degree of smoothing by the number of smearing steps (in parentheses the corresponding number of Laplace modes).

assigned to any cluster in a given configuration is adapted according to the resulting packing fraction f . Compared to considering cluster states being equivalent at equal q_{cut} , the watermark method reduces the noise from configuration to configuration. A *cluster* is then defined as a connected set of lattice sites lying above the watermark and having the same sign of the topological charge density. Choosing f we always have approximately the same number of clusters in all configurations. If we would compare configurations at fixed cutoff q_{cut} , there would be configurations with no clusters as well as configurations with many clusters.

Figure 3 (left) shows the changing cluster composition for various filtering methods, as function of f . In particular, the method denoted as *common* is interesting: Only those points are considered that are found by all three filtering methods. All curves show a pronounced power law for a small packing fraction f . A decrease of the curves signals the beginning of cluster percolation.

The remaining question is: does the exponent of the power law depend on the level of filtering? We found that the exponent of the power law describes a cluster composition that depends on the level of filtering. The right hand side plot of Figure 3 demonstrates this. The exponent indeed depends on the level of filtering. It changes most rapidly around 10 smearing steps, but reaches a plateau around 30. Data points for more than 30 smearing steps – or less than 6 Laplacian modes – do not make sense in this analysis since there would be so few clusters per configuration that we can hardly speak of a homogeneous cluster state. The horizontal mark in the right hand side plot in Figure 3 denotes the exponent that would correspond to the dilute instanton gas. From that plot, we can clearly see that the dilute instanton gas as a model for topological objects is excluded by our data.

5. Finite Temperature

Up to now, all results described zero temperature. Here we extend our investigation to the behavior of the topological lumps on both sides of the phase transition.

We used several ensembles above and below the critical temperature. Our set of ensembles consists of configurations with the same inverse coupling $\beta = 1.95$, with a spatial extent $N_s^3 = 20^3$ of the lattice and varying temporal size, $N_t = 4, 6, 8, 10, 12$. Each ensemble consists of 100 thermalized configurations. The ensembles with $N_t = 4, 6$ are clearly above the phase transition, $N_t = 10, 12$ are below the phase transition, and $N_t = 8$ is roughly at the phase transition.

The upper plots in Figure 4 show 2D-histograms of clusters. The abscissa shows the topological charge inside a given cluster, the ordinate shows the Polyakov loop averaged within the same cluster. The gray value indicates the height of a given bin. The top left plot is for 20 smearing steps and $N_t = 4$, the top right plot is for 20 smearing steps and $N_t = 12$. Clearly, the clusters themselves *do* feel the phase transition. The Polyakov loop inside a given cluster reflects the distribution of the global average of the Polyakov loop: in the deconfined phase the distribution is strongly peaked close to $L = \pm 1$, in the confined phase the distribution is wide, centered at 0.

The middle row of Figure 4 also shows 2D-histograms just like the top row, but the difference between the minimal and the maximal Polyakov loop within a cluster is shown. Above the phase transition this difference is small but below the phase transition larger clusters reveal a dipole-like structure in the local Polyakov loop. See also [9].

The lowest panel of Figure 4 shows the number of clusters vs. f for the five ensembles with $N_t = 4, \dots, 12$ at $\beta = 1.95$. We see that varying N_t , such that the ensembles are below or above the phase transition, seems to have no effect on the cluster composition as a function of f .

6. Conclusions

We conclude that all three filtering methods corroborate each other. If their parameters are mapped onto each other, they yield similar results. Especially smearing has often been criticized for producing arbitrary results. However, our results show – for moderate smearing with 10 to 30 smearing steps – that smearing keeps up with the other filtering methods. For this regime, the power law we found excludes the dilute instanton gas as a model for topological structures. Surprisingly, the power law survives the phase transition almost unchanged. This peculiar behavior requires further studies. The internal characteristics of the clusters — topological charge and Polyakov loop — strongly change with the onset of deconfinement.

References

- [1] F. Bruckmann *et al.* *Eur. Phys. J. A* **33** (2007) 333–338, [hep-lat/0612024](#).
- [2] C. Gattringer, E. M. Ilgenfritz, and S. Solbrig [hep-lat/0601015](#).
- [3] S. O. Bilson-Thompson, D. B. Leinweber, and A. G. Williams *Ann. Phys.* **304** (2003) 1–21, [hep-lat/0203008](#).
- [4] T. A. DeGrand, A. Hasenfratz, and T. G. Kovacs *Nucl. Phys.* **B520** (1998) 301–322, [hep-lat/9711032](#).

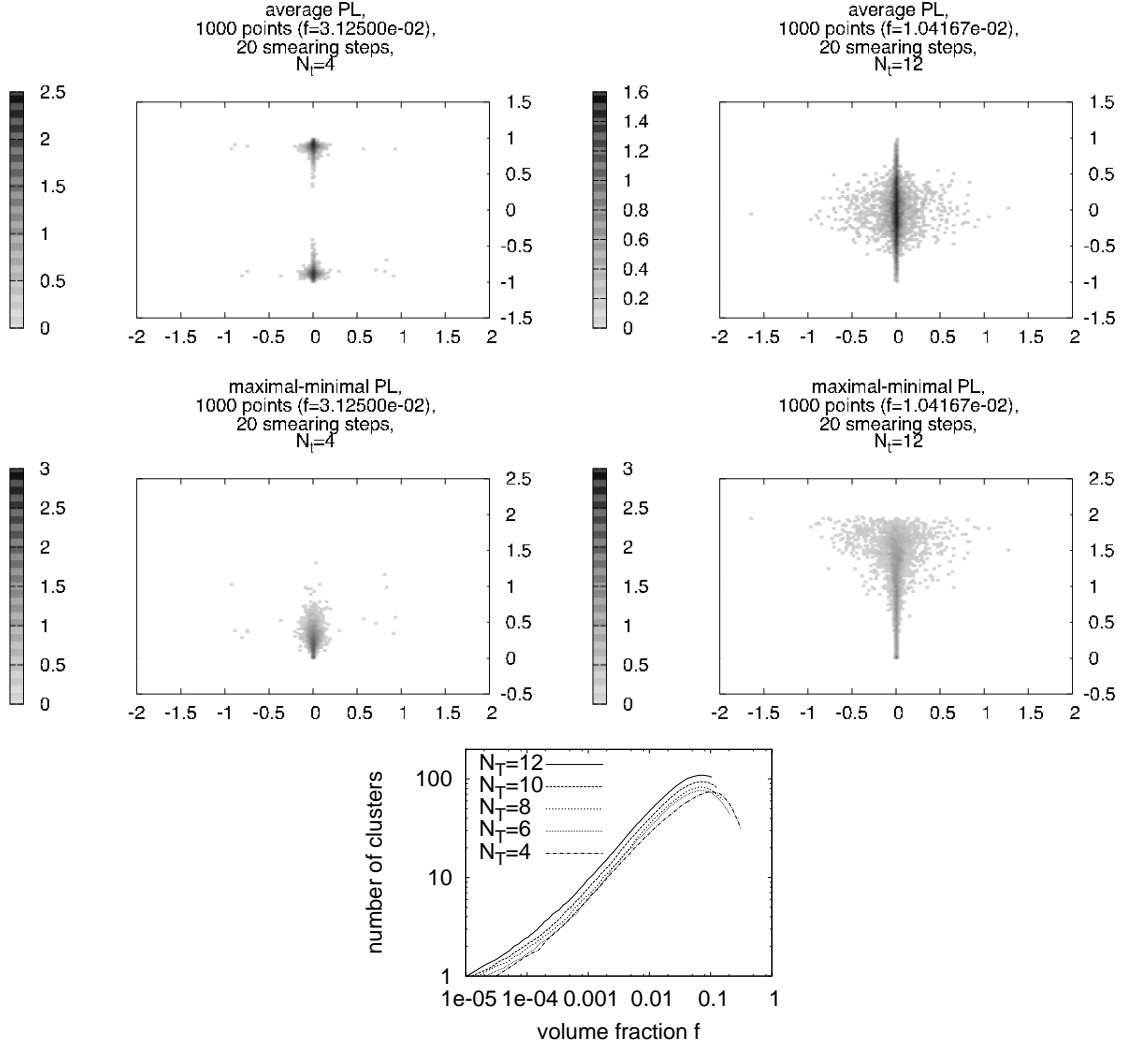


Figure 4: At the top, we show 2D-histograms of topological lumps. The abscissa indicates the total topological charge inside the cluster, the ordinate shows the averaged Polyakov loop through the cluster and the “grayness” shows the number of lumps in a given bin. The clusters indeed feel the phase transition. The middle row is similar to the top row, but shows the difference between the maximal and the minimal Polyakov loop within a cluster. At the bottom, we show in a double-log plot the number of clusters vs. packing fraction for finite temperature. The absolute number of the clusters varies, but this might be due to the varying total lattice volume. The slope of the distribution does apparently not change.

- [5] F. Bruckmann and E.-M. Ilgenfritz *Phys. Rev.* **D72** (2005) 114502, [hep-lat/0509020](#).
- [6] C. Gattringer and I. Hip *Phys. Lett.* **B480** (2000) 112–118, [hep-lat/0002002](#).
- [7] C. Gattringer *Phys. Rev.* **D63** (2001) 114501, [hep-lat/0003005](#).
- [8] T. A. DeGrand and A. Hasenfratz *Phys. Rev.* **D64** (2001) 034512, [hep-lat/0012021](#).
- [9] E. M. Ilgenfritz, B. V. Martemyanov, M. Müller-Preussker, and A. I. Veselov *Phys. Rev.* **D73** (2006) 094509, [hep-lat/0602002](#).